J Solid State Electrochem (2012) 16:937–944
DOI 10.1007/s10008-011-1462-0

ORIGINAL PAPER

Synthesis and characterization of macroporous $Li_3V_2(PO_4)_3$/C composites as cathode materials for Li-ion batteries

Xin Zhang · Suqin Liu · Kelong Huang · Shuxin Zhuang · Jun Guo · Tao Wu · Ping Cheng

Received: 30 March 2011 / Revised: 4 June 2011 / Accepted: 7 June 2011 / Published online: 18 June 2011

Abstract The macroporous $Li_3V_2(PO_4)_3$/C composite was synthesized by oxalic acid-assisted carbon thermal reaction, and the common $Li_3V_2(PO_4)_3$/C composite was also prepared for comparison. These samples were characterized by X-ray diffraction (XRD), scanning electron microscope (SEM), and electrochemical performance tests. Based on XRD and SEM results, the sample has monoclinic structure and macroporous morphology when oxalic acid is introduced. Electrochemical tests show that the macroporous $Li_3V_2(PO_4)_3$/C sample has a high initial discharge capacity (130 mAh g^{-1} at 0.1 C) and a reversible discharge capacity of 124.9 mAh g^{-1} over 20 cycles. Moreover, the discharge capacity of the sample is still 91.5 mAh g^{-1}, even at a high rate of 2 C, which is better than that of the sample with common morphology. The improvement in electrochemical performance should be attributed to its improved lithium ion diffusion coefficient for the macroporous morphology, which was verfied by cyclic voltammetry and electrochemical impedance spectroscopy.

Keywords Lithium vanadium phosphates · Macroporous · Li-ion batteries · Carbon thermal reaction

Introduction

Recently, lithiated transition metal phosphates such as $LiMPO_4$ (M=Fe, Co, Ni, and Mn) [1–6] and $Li_3M_2(PO_4)_3$ (M=Fe and V) [7–11] have been extensively investigated as positive materials for Li-ion battery. Among these materials, the monoclinic $Li_3V_2(PO_4)_3$ has attracted great interests due to its large theoretical capacity, high reversible capacity, and high operating voltage [12–15]. However, the poor electrical conductivity and slow lithium ion diffusivity hinder large-scale applications of this material.

Generally, to improve the electrical conductivity and lithium ion diffusivity of this kind of cathode material, coating with electrically conductive materials such as carbon [16–18] and metal doping [17, 19] have been extensively applied. Besides the methods mentioned above, optimizing the morphology of cathode materials is considered to be another effective way to improve the electrochemical performance. Doherty et al. [20] prepared porous $LiFePO_4$/C electrode material with an excellent discharge capacity, especially at high rate. Xiao et al. [21] synthesized Li_2FeSiO_4/C by a facile one-step technique. They found that both the capacity and cycling performance were greatly improved due to the porous morphology. Following this idea, it is thereby expected that optimizing the morphology of $Li_3V_2(PO_4)_3$/C materials would result in an improvement of its electrochemical performance.

In this study, the macroporous $Li_3V_2(PO_4)_3$/C composite was successfully synthesized by oxalic acid-assisted carbon thermal reaction. The structural properties and morphology of $Li_3V_2(PO_4)_3$/C composite as well as electrochemical properties were investigated.

Experimental

Synthesis and characterization

All the starting materials were analytically pure grade. At first, a stoichiometric amount of Li_2CO_3, V_2O_5, and $NH_4H_2PO_4$ and the desired amount of oxalic acid were

X. Zhang · S. Liu (✉) · K. Huang · S. Zhuang · J. Guo · T. Wu · P. Cheng
College of Chemistry and Chemical Engineering,
Central South University,
Changsha 410083, China
e-mail: sqliu2003@126.com

mixed. The molar ratio of Li_2CO_3:V_2O_5:$NH_4H_2PO_4$:$H_2C_2O_4$ is 3:2:6:12. Meanwhile, a certain amount of starch was employed here as a carbon source for reduction and coating. The mixture was initially dispersed in ethanol and then mixed intensively by ball-milling for 5 h. After that, the mixture was dried in a blast oven at 80 °C for 4 h. As follows, the precursor was preheated at 350 °C for 4 h and finally calcined at 800 °C for 8 h to obtain macroporous $Li_3V_2(PO_4)_3$/C composite (labeled as LVP-2) under flowing argon. For comparison, $Li_3V_2(PO_4)_3$/C composite (labeled as LVP-1) without oxalic acid as assistant was also prepared by the identical process.

An X-ray diffraction (XRD) of the product was carried on a RigaKu D/max2550VB$^+$ 18 kW from 10° to 60° using graphite-monochromatized CuKα radiation (40 kV, 250 mA). Both the morphologies and energy dispersive X-ray spectroscopy (EDS) of the as-prepared $Li_3V_2(PO_4)_3$/C particles were observed by a Hitachi S-4800 scanning electron microscope equipment. The surface area for samples was measured by the Brunauer–Emmett–Teller (BET) method using a surface area analyzer (Belsorp, Japan). The samples were assembled in CR2016 coin-type cells. The working electrode consisted of dispersing 85 wt.% as-prepared powder, 10 wt.% carbon black, and 5 wt.% polyvinylidene fluoride binder into the N-methylpyrrolidone solvent to form homogeneous slurry. The slurry was then cast onto an aluminum foil, and the coated electrodes were dried at 120 °C for 12 h in a vacuum. The CR2016 coin cells were assembled in an argon-filled glove box (Mbraun, Uni-lab, Germany) with a lithium foil as the counter electrode. The electrolyte was 1 M $LiPF_6$ in a mixture of EC–DMC–DEC (volume ratio of 1:1:1) electrolyte. The cells were galvanostatically charged and discharged between 3.0 and 4.3 V (voltage unit in this paper is versus Li/Li$^+$) at room temperature (25 °C) on the electrochemical test instrument (CT2001A, Wuhan Land Electronic Co. Ltd., China). Cyclic voltammetry measurements were performed using an electrochemical workstation (Shanghai Chenhua Instrument Co. Ltd., China) at a scan rate of 0.1 mV s^{-1} between 3.0 and 4.3 V. Electrochemical impedance spectroscopy (EIS) was recorded by the ZAHNER-IM6 electrochemical workstation (Germany) over the frequency range from 100 kHz to 100 mHz with an amplitude of 5 mV. The vanadium ion contents of the electrolytes were analyzed using an inductively coupled plasma (ICP) spectrometer (Thermo Fisher Scientific, 6500).

Results and discussion

X-ray diffraction

The XRD patterns of the LVP-1 and LVP-2 are shown in Fig. 1. All diffraction peaks are well indexed to be monoclinic structure with space group of $P2_1/n$ and no phase of impurity is detected in these patterns, which are consistent with the previous reports [9, 22]. And there are no obvious differences in the XRD patterns of the two samples. This suggests that the crystal structure of LVP-2 remained stable when the oxalic acid was added during preparation. And the EDX results as shown in Fig. 2c, d display that there is a carbon element in both samples.

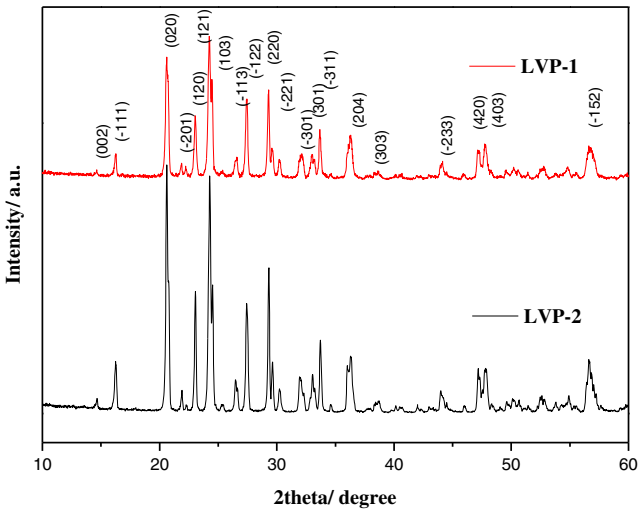

Fig. 1 XRD patterns of LVP-1 and LVP-2

SEM of $Li_3V_2(PO_4)_3$/C composite

Figure 2 presents the SEM images of the two samples. As Fig. 2a shows, LVP-1 appears the agglomeration of particles in an irregular shape. When the oxalic acid was introduced during preparation, bulky well-formed macroporous morphology in Fig. 2b is related to the vigorous evolution of gases by the oxalic acid anion degradation in the progress of calcination, which is in good agreement with Dominko et al. [23]. They thought the porous morphology was due to the formation of large quantity of gases during citrate anion degradation.

To illustrate the advantage of the macroporous morphology material, a model was built as shown in Fig. 3. For a bulk morphology material (Fig. 3a), the material contact with electrolytes mainly on the surface, little electrolytes can penetrate the material. Whereas in macroporous morphology material (Fig. 3b), the electrolytes permeate into the interior of the material and the electrolytes contact with the material sufficiently, which reduces the transportation distance of Li$^+$ and facilitates the diffusion of Li$^+$. Thus, it is beneficial to the electrochemical performance of the cathode material as mentioned in Refs. [24, 25].

To investigate the effect of carbon coating, the electronic conductivity of the samples were tested by a four-point probe method. The electronic conductivities of LVP-1 and

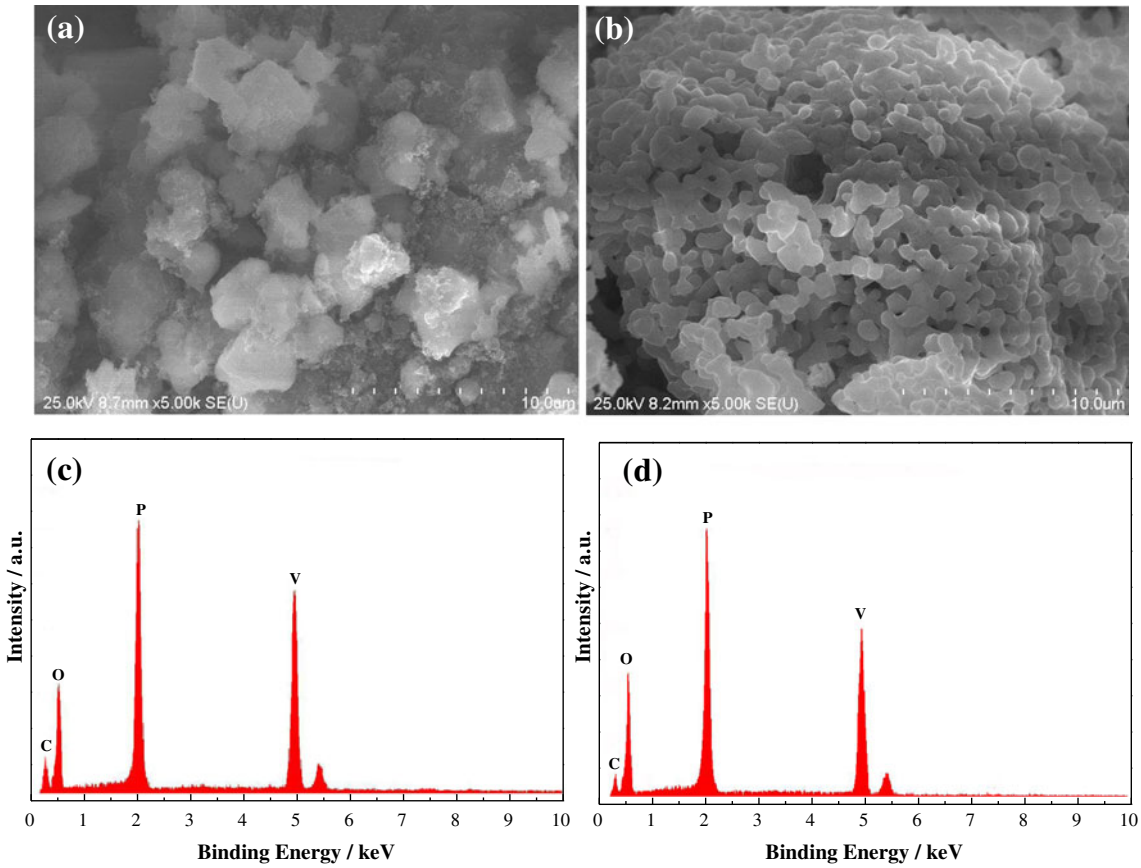

Fig. 2 SEM images of LVP-1 (**a**), LVP-2 (**b**) and EDS of LVP-1 (**c**) and LVP-2 (**d**)

LVP-2 are 4.79 and 5.23×10^{-3} S cm^{-1}, which are nearly five orders of magnitude greater than that of the carbon free $Li_3V_2(PO_4)_3$ (9×10^{-8} S cm^{-1}) [10]. Furthermore, the amount of residual carbon in LVP-1 and LVP-2 are 2.71 and 3.45 wt.%, respectively, which is measured by C-S 600 infrared carbon sulfur analyzer. The amount of residual carbon in LVP-2 is higher, which could be attributed to the reduction of oxalic acid. The difference of residual carbon in both samples has not seriously affected the electronic conductivity as the result of four-point probe method shows. It indicates that the effect of carbon coating on the electronic conductivity for both samples could be deemed to be equivalent.

Electrochemical performance at room temperature

The initial charge/discharge curves for LVP-1 and LVP-2 at 0.1 C in the potential range of 3.0–4.3 V are shown in Fig. 4. As it shows, both the samples exhibit three charge plateaus around 3.6, 3.7, and 4.1 V and the

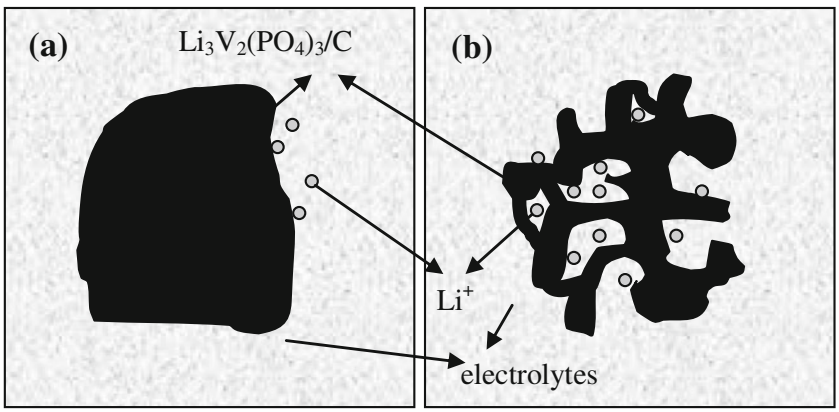

Fig. 3 Schematic presentation of the penetration of the electrolytes in LVP-1 (**a**) and LVP-2 (**b**)

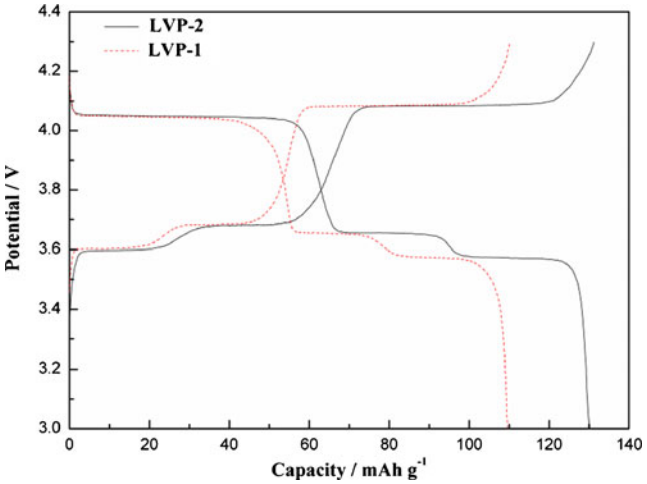

Fig. 4 The initial charge/discharge curves of LVP-1 and LVP-2

corresponding three discharge plateaus around 3.5, 3.6, and 4.0 V, which are identified as the two-phase transition process during the electrochemical reaction. The initial special discharge capacities for LVP-1 and LVP-2 are 109.5 and 130 mAh g^{-1}, respectively. Apparently, the initial discharge capacity of LVP-2 is much higher than that of LVP-1, which should be contributed to the effect of macroporous morphology.

The cycling performance of LVP-1 and LVP-2 at different rates were conducted and shown in Fig. 5. LVP-1 delivers the discharge capacity of 109.5, 92.6, 74.7, and 43.6 mAh g^{-1} at 0.1, 0.5, 1, and 2 C, respectively. For LVP-2, the corresponding discharge capacity is 130.0, 122.0, 112.4, and 91.5 mAh g^{-1}, respectively. Obviously, the discharge capacity decreases a little with an increasing charge/discharge rate.

It is observed that LVP-2 has higher discharge capacity and better cycling stability than that of LVP-1 at various rates. Especially in high rates such as at 2 C, LVP-2 shows much better cycling performance than that of LVP-1. The discharge capacity of LVP-2 achieves 85.1 mAh g^{-1} (93.00% of the initial discharge capacity) after 50 cycles, while that of LVP-1 is only 27.6 mAh g^{-1} after 50 cycles. Further, both the samples are applied again at 0.1 C after high rates. The first discharge capacity of LVP-2 is 124.2 mAh g^{-1}, which is 95.54% of the initial discharge capacity at 0.1 C before cycling at high rates. And the capacity retention is 95.09% after 20 cycles. The first discharge capacity and the capacity retention of LVP-1 are 101.8 mAh g^{-1} and 91.16%, which are less than that of the LVP-2.

The cycle efficiency of both samples during cycling at various rates is shown in Fig. 6. The LVP-2 holds high cycle efficiency during cycling. During 20 (at the rates 0.1and 0.5 C) and 50 (at the rates 1 and 2 C) cycles, the lowest cycle efficiencies are 96.08%, 96.39%, 97.33%, and 93.00%, respectively. After cycling at high rates and returning to cycle at 0.1 C again, the LVP-2 still has high cycle efficiency which is not lower than 95.09%, whereas the cycle efficiency of LVP-1 at various rates drops seriously. During 20 (at the rates 0.1 C and 0.5 C) and 50 (at the rates 1 C and 2 C) cycles, the lowest cycle efficiency are 93.06%, 90.28%, 78.98%, and 63.30%, respectively.

As the Figs. 5 and 6 has shown, both of the samples existing capacity fade during cycling, while the capacity retention of the LVP-2 at various rates is higher than that of LVP-1. The irreversible capacity of lithium ion battery may be caused by many reasons such as the change of structure and powdering during charge/discharge, overcharge, and overdischarge [9, 26, 27]. The specific surface area of LVP-1 and LVP-2 which is measured by BET method are 2 and 35 m^2 g^{-1}, respectively. According to the mosaic model [28], the bulk morphology of LVP-1 is adverse to the efficiency of active materials, leading to the irreversible

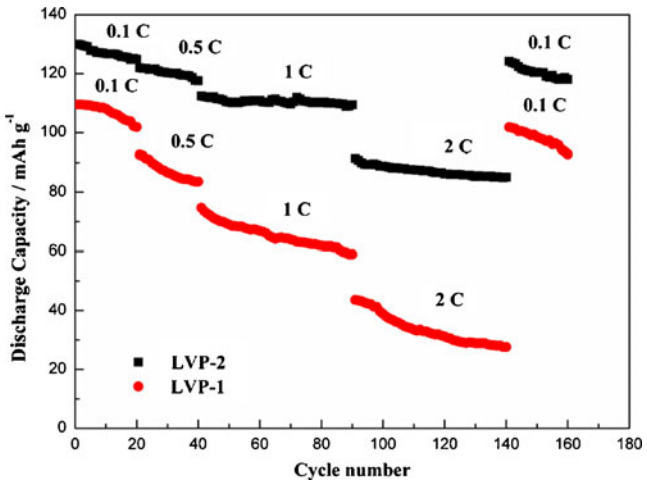

Fig. 5 Cycling performances of LVP-1 and LVP-2 at different rates

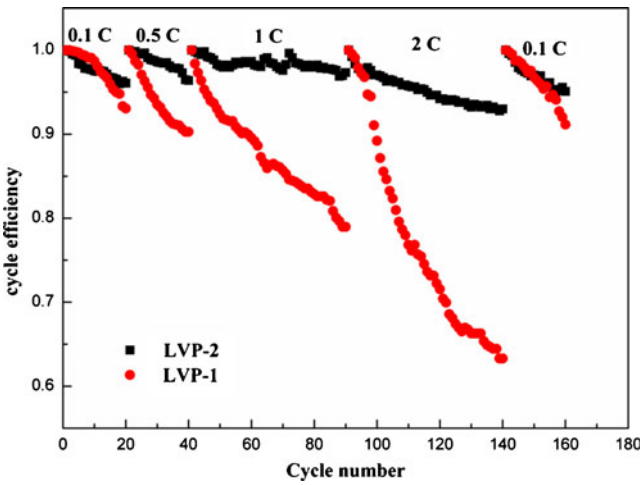

Fig. 6 The cycle efficiency of both samples LVP-1 and LVP-2 at various rates

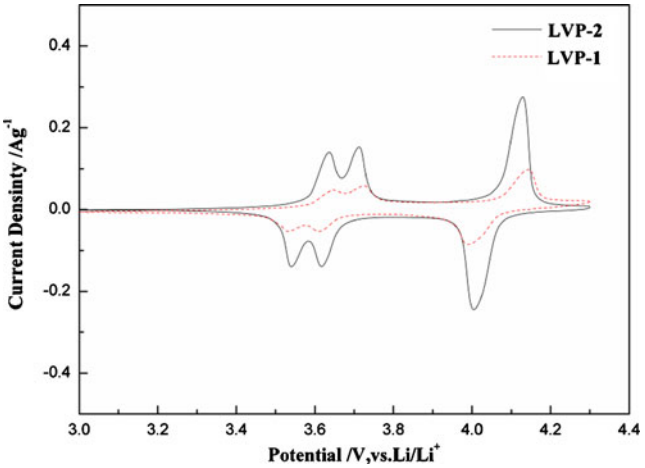

Fig. 7 Cyclic voltammograms of LVP-1 and LVP-2 at 0.1 mV/s between 3.0 and 4.3 V in the second cycle

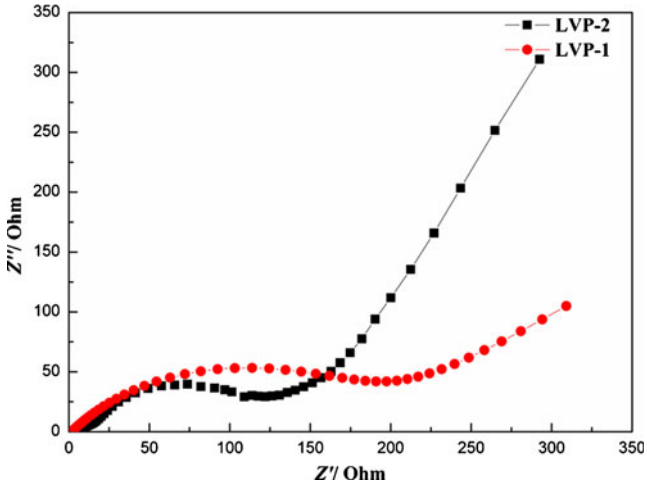

Fig. 8 Impedance spectra of LVP-1 and LVP-2 at the charge potential of 4.3 V during the second cycle

capacity, especially at high rates. While the large surface area of material favors to shorten diffusion pathway and get the diffusion of ionic easily, resulting in excellent electrochemical performance [29–31].

The cyclic voltammograms of both samples at a scan rate of 0.1 mV s^{-1} is presented in Fig. 7. There are three pairs of redox peaks with the oxidation peaks located at about 3.63, 3.71, and 4.13 V and the corresponding reduction peaks at about 3.54, 3.61, and 4.00 V, respectively, which agree with the charge/discharge curves in Fig. 3. The appearance of redox peaks indicates the reversible Li^+ de-intercalation and intercalation in solid phase. Moreover, the current density of LVP-2 electrode is higher than that of the LVP-1 electrode. It is well known that the relationship between the current density and the diffusion coefficient of lithium ions i_p is complied with the following formula [32]:

$$i_p = 2.6 \times 10^5 n^{3/2} C_0 D^{1/2} v^{1/2}$$

where n is the number of electrons transferred per molecule during the intercalation, C_0 is the concentration of lithium ions, D is the diffusion coefficient of lithium ions, and v is the scan rate. Since i_p is proportional to $D^{1/2}$, it is easily inferred that the Li^+ diffusion coefficient of LVP-2 is higher than that of the LVP-1. Meanwhile, the potential differences between anodic and cathodic peaks are smaller in LVP-2 electrode, suggesting the faster transport of electrons and ions in the LVP-2 electrode case.

To further understand the reason for a better electrochemical performance of LVP-2, Nyquist plots of both the samples are recorded in Fig. 8. The half-cells were charged to 4.3 V at the second cycle and kept at that voltage for 3 h before EIS tests. As shown, both the EIS curves are composed of a semicircle and a linear part in the frequency range from 100 kHz to 10 mHz. The high frequency semicircle is attributed to the migration of Li^+ through the SEI film which represents the charge transfer resistance. The inclined line in the low frequency range represents the Warburg impedance, which is associated with the diffusion of Li^+ in the bulk of the electrode material. It is well known that the charge transfer resistance is proportional to the diameter of semicircle in high frequency region and the Warburg impedance is inversely proportional to the slope of the inclined line in the low frequency. As shown in Fig. 8, the diameter of semicircle for LVP-2 is obviously smaller than that of the LVP-1, indicating that the charge transfer is more favorable on LVP-2 electrode (the charge transfer resistances of LVP-1 and LVP-2 are 256.3 and 183.0 Ω, respectively). And the slope of the low frequency inclined line of LVP-2 is larger than that of LVP-1, indicating that the lithium ion diffusion coefficients of LVP-2 may be higher than that of LVP-1.

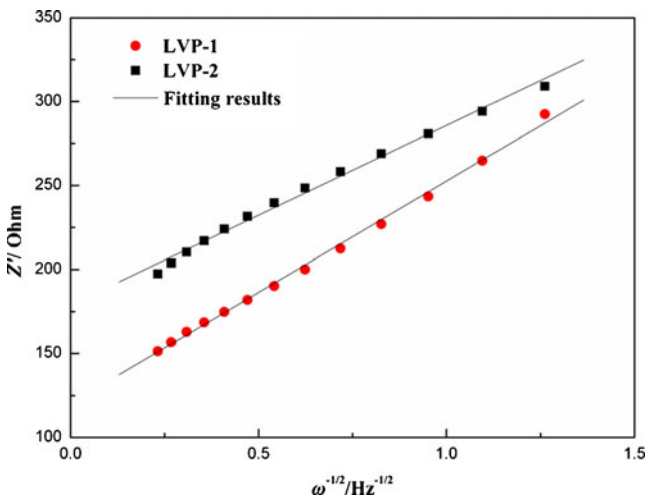

Fig. 9 The relationship between $Z'$and square root of frequency ($\omega^{-1/2}$) in the low-frequency region of LVP-1 and LVP-2

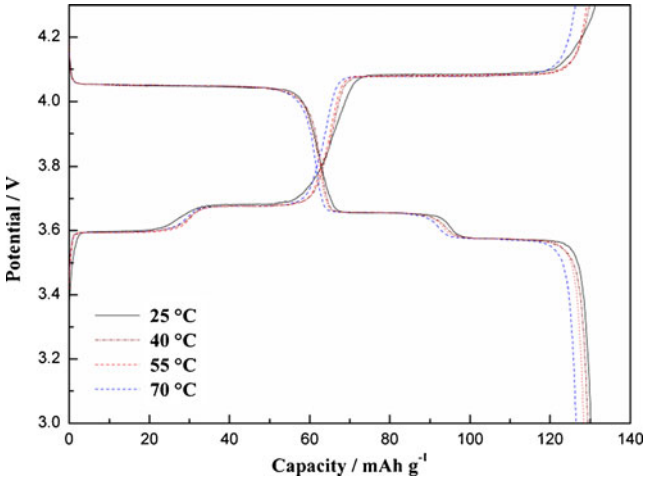

Fig. 10 The initial charge/discharge curves of macroporous material after aging at different temperature

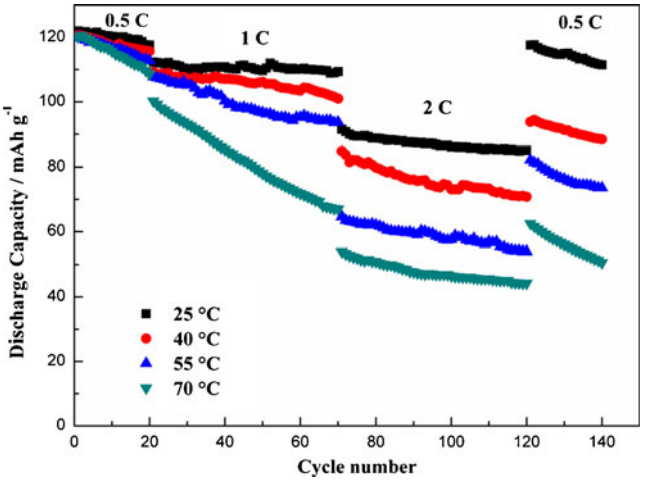

Fig. 12 Rate capability of $Li_3V_2(PO_4)_3$/C samples at different test temperatures

To further investigate the difference of the lithium ion diffusion coefficients (D) between LVP-1 and LVP-2, they are calculated according to the following equation [33]:

$$D = R^2T^2/2A^2n^4F^4C^2\sigma^2 \quad (1)$$

Where R is the gas constant, T is the absolute temperature, A is the surface area of the cathode, n is the number of electrons per molecule during oxidization, F is the Faraday constant, C is the concentration of lithium ion, and σ is the Warburg factor which has relationship with Z':

$$Z' = R_D + R_L + \sigma\omega^{-1/2} \quad (2)$$

Figure 9 shows the relationship between Z' and square root of frequency ($\omega^{-1/2}$) in the low-frequency region. The diffusion coefficient of lithium ion is calculated based on Eqs. 1 and 2. The calculated lithium ion diffusion coefficients of LVP-1 and LVP-2 are 9.24×10^{-12} and 1.42×10^{-11} cm^2 s^{-1}, respectively. It is obvious that the lithium ion diffusion coefficient drastically increases, implying that the insertion/extraction of Li^+ in LVP-2 electrode is much easier. From the EIS analysis above, the LVP-2 has the lower charge transfer resistances and higher lithium ion diffusion coefficient, which led to the excellent electrochemical performance of LVP-2 in high rates [34, 35]. The EIS results further confirmed that the modified electrochemical performance is associated with the bulky well-formed macroporous morphology of LVP-2.

Electrochemical performance at elevated temperatures

In the previous investigation, LVP-2 with macroporous morphology exhibits an excellent electrochemical performance at room temperature. Herein, the performance of

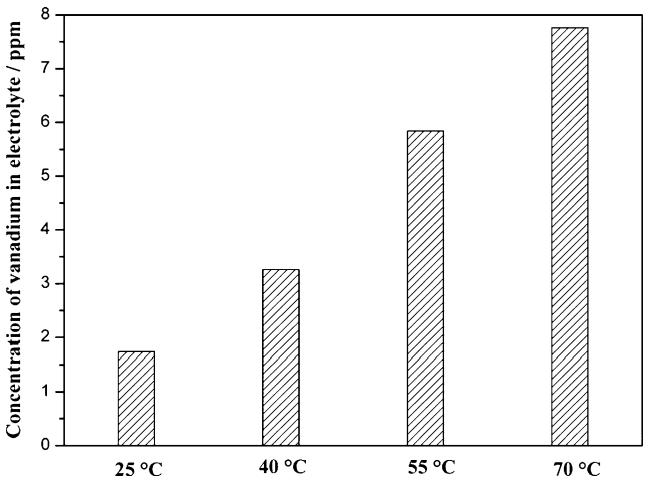

Fig. 11 Concentration of vanadium ion in electrolyte after aging at different temperature

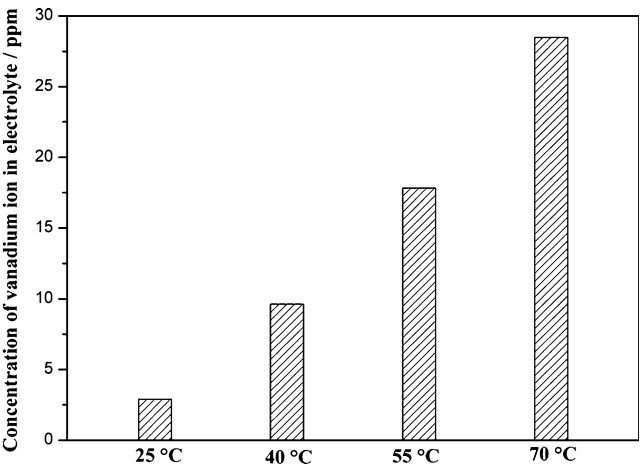

Fig. 13 Concentration of vanadium ion in electrolyte after rate performance testing at different temperatures

LVP-2 at elevated temperature is evaluated. The charge/discharge test was carried out after aging at 25, 40, 55, and 70 °C for about 3 days. The initial charge/discharge curves of LVP-2 at 0.1 C are shown in Fig. 10. The initial discharge capacities of the samples at 25, 40, 55, and 70 °C are 130.0, 129.4, 128.3, and 126.5 mAh g^{-1}, respectively. It is suggested that when the operation temperature is elevated, the initial discharge capacity of LVP-2 drops down slightly.

To investigate the reason for the fading of the initial discharge capacity, the vanadium ion concentration in electrolyte was detected by ICP analysis. As shown in Fig. 11, the vanadium concentration in the electrolyte after testing at different operation temperatures are 1.73, 3.26, 5.84, and 7.76 ppm, respectively, indicating that the vanadium ion concentration in electrolyte increased with the operation temperature elevating.

The discharge capacity and the cycle performance of the LVP-2 at different rates were shown in Fig. 12. As the temperature was elevating, the discharge capacity and the cycle performance of the samples decreased progressively. The initial discharge capacities of LVP-2 at 25 °C are 122, 112.4, and 91.5 mAh g^{-1} at 0.5, 1, and 2 C, respectively, which are higher than that of the 70 °C sample (120.1, 100.2, and 53.9 mAh g^{-1}). After 20 (at 0.5 C) and 50 cycles (at 1 and 2 C), the capacity retentions of LVP-2 at 25 °C are 96.39%, 97.33%, and 93.01%, which are higher than that at other temperatures. Even when 0.5 C is applied again, the LVP-2 at 25 °C present the best reproducibility in the all operation temperatures. The reason for the fading of the electrochemical performance with the elevation of operation temperature may be attributed to the dissolution of the active material. Then, the concentrations of vanadium ions in the electrolytes operating at different temperatures were determined by ICP. As shown in Fig. 13, the concentration of vanadium ions in electrolyte increased with the temperature rising. It indicates that more active materials dissolve into electrolyte with the operation temperature increasing. Fu et al. [36] and Amine et al. [37] found that the dissolution of transition metal cations was adverse to their electrochemical performance.

The results suggest that some further work need to be done to improve the high temperature performance of the LVP-2. However, the excellent electrochemical performance of the LVP-2 at room temperature indicates that it is a very promising cathode material for Li-ion battery.

Conclusions

In summary, $Li_3V_2(PO_4)_3$/C composite with macroporous morphology was successfully synthesized by oxalic acid-assisted carbon thermal reaction. The XRD results show that no other impurity is detected. Compared with LVP-1, LVP-2 shows better reversible capacity and improved rate capability, which is due to the higher lithium ion diffusion coefficient for its macroporous morphology. LVP-2 exhibits an initial discharge capacity of 130.0, 122.0, 112.4, and 91.5 mAh g^{-1} as it is discharged at 0.1, 0.5, 1, and 2 C rates, respectively. After 20 (at the rates 0.1 and 0.5 C) and 50 (at the rates 1 and 2 C) cycles, the corresponding discharge capacity values are about 124.9, 117.6, 109.4, and 85 mAh g^{-1}, respectively. And the cell retains 96.08%, 96.39%, 97.33%, and 93.00% of its initial discharge capacity. Therefore, the as-prepared macroporous $Li_3V_2(PO_4)_3$/C with high capacity and good cyclic stability is a very promising cathode material for Li-ion battery.

Acknowledgments This work was supported by the National Natural Science Foundation of China (No. 51072234), Graduate Degree Thesis Innovation Foundation of Central South University (2010ssxt014).

References

1. Padhi AK, Nanjundaswamy KS, Goodenough JB (1997) J Electrochem Soc 144:1188–1194
2. Bramnik NN, Bramnik KG, Buhrmester T, Baehtz C, Ehrenberg H, Fuess H (2004) J Solid State Eletrochem 8:558–564
3. Zhang M, Jiao LF, Yuan HT, Wang YM, Guo J, Zhao M, Wang W, Zhou XD (2006) Solid State Ionics 177:3309–3314
4. Li HH, Jin J, Wei JP, Zhou Z, Yan J (2009) Electrochem Commun 11:95–98
5. Koltypin M, Aurbach D, Nazar L, Ellis B (2007) J Power Sources 174:1241–1250
6. Meethong N, Kao YH, Tang M, Huang HY, Carter WC, Chiang YM (2008) Chem Mater 20:6189–6198
7. Sato M, Tajimi S, Okawa H, Uematsu K, Toda K (2002) Solid State Ionics 152:247–251
8. Wang LN, Li ZC, Xu HJ, Zhang KL (2008) J Phys Chem C 112:308–312
9. Saïdi MY, Barker J, Huang H, Swoyer JL, Adamson G (2003) J Power Sources 119–121:266–272
10. Yin SC, Strobel PS, Grondey H, Nazar LF (2004) Chem Mater 16:1456–1465
11. Mateyshina YG, Uvarov NF (2011) J Power Sources 196:1494–1497
12. Yin SC, Grondey H, Strobel P, Anne M, Nazar LF (2003) J Am Chem Soc 125:10402–10411
13. Morgan D, Ceder G, Saïdi MY, Swoyer J, Huang H, Adamson G (2002) Chem Mater 14:4684–4693
14. Gaubicher J, Wurm C, Goward G, Masquelier C, Nazar L (2000) Chem Mater 12:3240–3242
15. Sato M, Ohkawa H, Yoshida K, Saito M, Uematsu K, Toda K (2000) Solid State Ionics 135:137–142
16. Li YZ, Zhou Z, Ren MM, Gao XP, Yan (2006) Electrochim Acta 51:6498–6502
17. Yu F, Zhang JJ, Yang YF, Song GZ (2010) J Solid State Electrochem 14:883–888
18. Ren MM, Zhou Z, Gao XP, Peng WX, Wei JP (2008) J Phys Chem C 112:5689–5693
19. Yang SY, Zhang S, Fu BL, Wu Q, Liu FL, Deng C (2010) Effects of Cr doping on the electrochemical performance of $Li_3V_2(PO_4)_3$ cathode material for lithium ion batteries. J Solid State Electrochem. doi:10.1007/s10008-010-1255-x

20. Doherty CM, Caruso RA, Smarsly BM, Adelhelm P, Drummond CJ (2009) Chem Mater 21:5300–5306
21. Fan XY, Yan L, Wang JJ, Lei G, Peng Z, Li DL, Ling H, Sun SG (2010) J Alloys Compd 493:77–80
22. Huang H, Yin SC, Kerr T, Taylor N, Nazar LF (2002) Adv Mater 14:1525–1528
23. Dominko R, Goupil JM, Bele M, Gaberscek M, Remskar M, Hanzel D, Jamnik J (2005) J Electrochem Soc 152:A858–A863
24. Lin B, Wen ZY, Wang XY, Liu Y (2010) J Solid State Electrochem 14:1807–1811
25. Koike S, Tatsumi K (2007) J Power Sources 174:976–980
26. Aurbach D, Markovsky B, Rodkin A, Cojocaru M, Levi E, Kim HJ (2002) Electrochim Acta 00:1–13
27. Chen JT, Zhou HH, Chang WB, Ci YX (2003) Acta Phys-Chim Sin 19:278–282
28. Andersson AS, Thomas JO (2001) J Power Sources 97–98:498–502
29. Shen LF, Yuan CZ, Luo HJ, Zhang XG, Xu Ke, Xia YY (2010) J Mater Chem 20:6998–7004
30. Dominko R, Bele M, Gaberscek M, Remskar M, Hanzel D, Goupil JM, Pejovnik S, Jamnik J (2006) J Power Sources 153:274–280
31. Prakash AS, Manikandan P, Ramesha K, Sathiya M, Tarascon JM, Shukla AK (2010) Chem Mater 22:2857–2863
32. Bard AJ, Faulkner LR (1980) Electrochemical methods. Wiley, New York, p 213
33. Bard AJ, Faulkner LR (2001) Electrochemical methods. Wiley, New York, p 231
34. Sun CS, Zhang Y, Zhang XJ, Zhou Z (2010) J Power Sources 195:3680–3683
35. Rui XH, Li C, Chen CH (2009) Electrochim Acta 54:3374–3380
36. Fu MH, Huang KL, Liu SQ, Liu JS, Li YK (2010) J Power Sources 195:862–866
37. Amine K, Liu J, Belharouak I (2005) Electrochem Commun 7:669–673